HHS Public Access

Author manuscript

Lab Chip. Author manuscript; available in PMC 2015 October 19.

Published in final edited form as:

Lab Chip. 2013 April 7; 13(7): 1247–1256. doi:10.1039/c3lc41330f.

External cavity laser biosensor†

Chun Ge[a], **Meng Lu**[a], **Sherine George**[b], **Timothy A. Flood Jr.**[d], **Clark Wagner**[a], **Jie Zheng**[a], **Anusha Pokhriyal**[c], **J. Gary Eden**[a], **Paul J. Hergenrother**[d], and **Brian T. Cunningham**[a,b]

[a]Department of Electrical and Computer Engineering, University of Illinois at Urbana-Champaign, Urbana, Illinois, 61801, USA. bcunning@illinois.edu

[b]Department of Bioengineering, University of Illinois at Urbana-Champaign, Urbana, Illinois, 61801, USA

[c]Department of Physics, University of Illinois at Urbana-Champaign, Urbana, Illinois, 61801, USA

[d]Department of Chemistry, University of Illinois at Urbana-Champaign, Urbana, Illinois, 61801, USA

Abstract

Utilizing a tunable photonic crystal resonant reflector as a mirror of an external cavity laser cavity, we demonstrate a new type of label-free optical biosensor that achieves a high quality factor through the process of stimulated emission, while at the same time providing high sensitivity and large dynamic range. The photonic crystal is fabricated inexpensively from plastic materials, and its resonant wavelength is tuned by adsorption of biomolecules on its surface. Gain for the lasing process is provided by a semiconductor optical amplifier, resulting in a simple detection instrument that operates by normally incident noncontact illumination of the photonic crystal and direct back-reflection into the amplifier. We demonstrate single-mode, biomolecule-induced tuning of the continuous-wave laser wavelength. Because the approach incorporates external optical gain that is separate from the transducer, the device represents a significant advance over previous passive optical resonator biosensors and laser-based biosensors.

Introduction

Since the introduction of SPR biosensors,[1] a variety of optical devices and phenomena have been adapted to the task of detecting biochemical interactions without the use of labels. Of the first generation of detection methods, which include ellipsometers,[2] interferometers,[3–9] waveguides,[10] grating couplers,[11–13] and holograms,[14] SPR has gained the most widespread commercial acceptance.[1,15–17] A tremendous number of label-free assays for every conceivable type of biological analyte have been demonstrated.[18,19] Yet, there has always been a desire to extend the limits of detection of label-free assays to lower concentrations and to increase the signal-to-noise ratio for observation of the lowest concentrations or the smallest molecules. Applications in pharmaceutical high-throughput screening, pathogen

†Electronic supplementary information (ESI) available. See DOI: 10.1039/c3lc41330f

Correspondence to: Brian T. Cunningham.

detection, and life science research all demand a challenging combination of low cost, robustness, high sensitivity, resolution, and high-throughput.

More recently, label-free biosensor approaches derived from dielectric-based optical resonators have been demonstrated. Optical resonators can efficiently couple energy within their structure for a narrow range of wavelengths (for a fixed coupling angle), or conversely for a narrow range of angles (for a fixed wavelength). At the resonant wavelength/angle combination, the electromagnetic field energy associated with the light is temporarily stored within the resonator and in the medium surrounding the resonator. The magnitude of the evanescent field extending from the resonator and into liquid media drops exponentially with distance as one moves away from the surface of the resonator, and it is within this evanescent field region that biomolecules adsorbed to the surface of the resonator have the capacity to modulate the resonant wavelength/angle coupling condition though their intrinsic dielectric permittivity. Therefore, an important design goal for resonant optical biosensors is to concentrate the electromagnetic field outside of the resonant structure itself to increase the extent of interaction with adsorbed biomolecules.[20] Optical resonators that simply reflect or transmit light from an external source are classified as passive devices because all the illumination is provided externally.

New designs for resonant optical biosensors to date have focused on the development of passive dielectric structures with higher *Q*-factor, where $Q = \lambda_0/\Delta\lambda$, and $\Delta\lambda$ represents the spectral width (full width at half-maximum, FWHM) of the resonant mode at wavelength λ_0. Devices such as these, including photonic crystals,[21,22] whispering gallery mode spheres,[23–27] microrings,[28–30] liquid-core optical fibers,[31] and microdisks[32,33] have demonstrated impressive *Q*-factors due to the ability to strongly confine light within a high refractive index dielectric cavity. A narrower resonant spectrum results in the ability to measure small resonant wavelength shifts with greater accuracy, thus reducing limits of detection (LOD).[34] A widely adopted means for comparing performance between resonant optical biosensors is to calculate a figure of merit (FOM) that incorporates the sensitivity of the sensor (the magnitude of a measured quantity change) and the resolution for measuring small changes in that quantity.[35] The sensitivity of optical biosensor methods can be compared through their sensitivity to changes in the refractive index of a bulk medium deposited on their surface. The "bulk refractive index shift coefficient" defined as $S_b = \Delta\lambda/\Delta n_b$ characterizes how much the resonant wavelength of a sensor shifts, but it does not tell much about the smallest wavelength shift that can be resolved. On the other hand, the resolution strongly depends on the *Q*-factor of the resonance. Therefore, a FOM that combines sensitivity and resolution metrics can be defined as $\text{FOM} = S_b \times Q$. Table S1 (ESI[†]) compares FOM from a variety of optical resonator biosensor technologies.

While high *Q*-factor passive resonators can demonstrate excellent resolution, as the *Q*-factor increases, it becomes increasingly difficult to couple light into and out of the resonator, resulting in requirements for nanometer-level precision for positioning of optical fibers or waveguides to the resonator perimeter. In addition, several of these approaches require a high-precision tunable laser as the illumination source, resulting in systems that seem

[†]Electronic supplementary information (ESI) available. See DOI: 10.1039/c3lc41330f

difficult to multiplex to large numbers of sensors or a miniature/low-cost detection instrument. Importantly, improved resolution (through higher *Q*-factor) is accompanied by lower sensitivity, as resonant modes are mostly confined within the solid dielectric medium.

Recently, in order to address the difficulties encountered by high-*Q* passive resonator biosensors while maintaining merits such as improved resolution, the idea of active resonator laser biosensors has been proposed. Several laser-based label-free biosensors have been demonstrated, such as the distributed feedback laser biosensor by Lu *et al*. in 2008,[36] the photonic crystal laser biosensor by Kita *et al*. in 2008,[37] the optical fluidic laser by Sun *et al*. in 2010[38] and the microtoroid laser biosensor by He *et al*. in 2011.[39] The motivation for all these approaches is to improve the limit of detection by generating a high intensity and narrow wavelength output through the process of stimulated emission, compared to what is achievable with passive resonators. Although these laser biosensors have demonstrated exciting capabilities, there are several shortcomings shared by all of them that hinder their practical application for low-cost, high sensitivity, high throughput label-free biosensing. These include a very limited effective sensing area, expensive and low-throughput fabrication, the requirement for a large pump laser, and delicate calibration/coupling processes. Such characteristics significantly effect the sensor's dynamic range, increase the sensor chip cost and system volume, and reduce the detection throughput, rendering these methods inappropriate for low-cost, disposable sensors as single-use items for point-of-care diagnostic tests or for high-throughput pharmaceutical screening.

Here, we describe for the first time an alternative laser-based label-free optical biosensor approach that maintains the high resolution of laser biosensors while addressing the aforementioned shortcomings. The key innovation in our work is the introduction of gain from a source external to the sensor itself, resulting in a very robust detection system that allows low-cost, large area transducer/sensing chips, noncontact optical coupling, a compact/inexpensive electrical pump source, CW operation, and multiplexing – while at the same time achieving high sensitivity, large dynamic range, and the ability to measure very small wavelength shifts. In light of previous label-free biodetection approaches, and laser-based biosensing in particular, the approach presented in this paper represents a substantially important advance.

The novel element of our approach is the utilization of external optical gain, so as to realize an active optical cavity that achieves narrow bandwidth continuous wave light output *via* the process of stimulated emission. We use a photonic crystal (PC) resonant reflector surface as the transducer upon which biological material is adsorbed, which also serves as the wavelength selective mirror of the external cavity laser (ECL). As shown in Fig. 1, an optical fiber-coupled traveling-wave semiconductor optical amplifier (SOA) is used as the gain media, which illuminates the PC at normal incidence. The PC reflects a narrow band of wavelengths through the optical fiber, and back into the SOA to establish a laser cavity whose emission wavelength is tuned by the adsorption of biomaterial on the PC surface. Importantly, the smooth gain spectrum of the SOA and the length of the external cavity (determined by the length of the optical fiber) result in apparently continuous tuning of the lasing wavelength without abrupt hops between modes. The FOM of this approach, as shown in Table S1,[†] is greater than previously published passive resonator biosensors due to

the high *Q*-factor of the ECL emission (2.8×10^7) and the high refractive index sensitivity of the PC surface.

Tunable ECLs have generated considerable interest in optical communications, atomic laser spectroscopy, and environmental monitoring since the introduction of the first external cavity diode laser in 1964[40] and the first tunable systems afterward.[41,42] The typical tunable ECL system comprises a semiconductor laser diode or an SOA with an anti-reflection (AR) coating on at least one facet, a collimator for coupling the output of the diode to the external cavity, and an external mode-selection filter, as described in a recent textbook[43] and review.[44] Through the insertion of a wave-length-selective element into the system, an ECL configuration permits emission of a single-mode with a linewidth that is considerably less than that of a laser diode.[44] A detailed discussion of the factors that impact ECL wavelength stability and previously realized tunable ECL systems is included in the ESI.† This work represents the first instance of an ECL system being utilized as a biosensor.

Materials and methods

External cavity laser biosensor design

The sensor surface is a one-dimensional (1D) PC comprising a low refractive index, ultra-violet curable polymer (UVCP) periodic grating (Λ = 550 nm, $t_{grating}$ = 170 nm) coated with a high refractive index thin film of TiO_2 (n = 2.35, t_{TiO2} = 120 nm) that is designed to provide a resonant reflection near λ = 855 nm when covered with water. The PC sensor used in the study is engineered to operate with aqueous media on its surface. It is fabricated on a flexible plastic substrate using nanoreplica molding to form the grating structure, as described in our previous work.[45] Importantly, the PC sensor surface can be inexpensively manufactured over large surface areas to produce biosensors in a standard microplate format, for compatibility with automated liquid handling formats used for high-throughput applications.

The detection instrument comprises an SOA, two polarization maintaining single-mode optical fibers, a near-infrared (NIR) mirror, and an instrument for measuring laser wavelength. The SOA (SAL-372, Superlum Inc., λ_0 = 850 nm and a 3-dB bandwidth of $\Delta\lambda$ = 40 nm) has both edge facets coated with anti-reflection layers ($R < 10^{-3}$) with a tilted waveguide design to obtain a gain ripple as low as 0.2 dB.[46] Each end facet of the SOA is coupled to a single-mode polarization maintaining fiber with a length of 1 m.

The output of one side of the SOA is reflected against a mirror, while the other end directs light through a collimating lens against the PC at normal incidence. A portion of the lasing emission energy is directed by a 98 : 2 beam splitter to a detection instrument such as a spectrometer or interferometer. Theoretically, the ECL biosensor detection limit is ultimately set by the mode density or the free spectral range (FSR) of the ECL cavity. The cavity mode spacing is given by $\Delta\lambda_m \approx \frac{\lambda^2}{2(n_0 l_0 + n_g l_g + n_{\mathrm{SOA}} l_{\mathrm{SOA}})}$, where m is the mode number, λ_m is the m^{th} resonant wavelength, λ is the center wavelength, and n_0, n_g, n_{SOA}, l_0, l_g, l_{SOA} are the effective refractive index and length of the air, single-mode fiber, and the SOA cavity, resulting in a cavity length that is dominated by the length of the optical fiber.

By using two 1 m single-mode fibers, a longitudinal mode spacing of 0.08 pm is estimated, representing the smallest increment in wavelength shift that can be obtained. Our ECL system achieves single-mode operation by the same mechanism as normal grating-stabilized ECL systems, where the grating also reflects back a range of wavelengths, which is much wider than the FSR of the cavity. To enable single-mode operation, we set the injection current at 60 mA, a value just above the lasing threshold (48 mA). Under this condition, only the PC reflection peak and a narrow range of wavelength around the peak will be efficiently coupled into the single-mode fiber and the gain chip within the acceptance angle of the waveguide. The coupled light gets amplification inside the gain chip multiple times, depending on the *Q*-factor of the cold cavity. This amplification process will transfer the initially relatively wide reflection peak into a much narrower peak. Then, the lasing wavelength is determined by the longitudinal mode that first achieves the threshold condition.

As the ECL biosensor resonates, high intensity electromagnetic standing waves are established at the PC-media interface. Adsorption of biomolecules tunes the resonant wavelength of the PC, which subsequently tunes the emission wavelength of the ECL. While the PC is a passive optical resonator with modest *Q*-factor ($Q \sim 1000$), its interaction with the gain provided by a semiconductor optical amplifier through the formation of a resonant cavity results in an active optical resonator with an extremely high *Q* ($Q \sim 2.8 \times 10^7$) through the stimulated emission process, while retaining high sensitivity. The ECL biosensor generates single-mode, continuous-wave laser emission whose wavelength is tunable over a wide range by adsorption of biomaterial on the surface of the PC, and thus exhibits large dynamic range. This arrangement combines the high sensitivity of the PC passive resonator with the high resolution of the external cavity laser emission.

Characterization of the ECL

The reflection spectrum of the PC, the spontaneous emission spectrum of the SOA, and the laser emission spectrum of the ECL are shown together in Fig. 2(a). The PC exhibits a resonance peak with a 3-dB bandwidth of $\Delta\lambda = 2$ nm. Using a spectrometer to measure the ECL emission spectrum (IHR550, Horiba Jobin Yvon), the width of the lasing peak is at least as narrow as $\Delta\lambda = 30$ pm, as limited by the wavelength resolution of the spectrometer (with a resolution of 20 pm). To more accurately measure the *Q*, a scanning Fabry-Perot cavity interferometer with a resolution of 7.5 MHz was used. The interferogram is shown in Fig. 2(b) and 2(c). Fig. 2(b) is a FSR plot, which is used to calibrate the time-base of the oscilloscope. A *Q*-factor of 2.8×10^7 is determined at a center wavelength of $\lambda_0 \sim 853$ nm. It should be noted that all the *Q* measurement data was acquired with sensor surface coated with deionized water, as the photonic crystal sensor used in the study is engineered to operate with aqueous media on its surface. Water absorption near 850 nm is as small as 0.04 cm^{-1}, which is one reason why our PC is designed to operate at NIR wavelengths. The intense and narrow linewidth emission of the ECL laser sensor is able to resolve extremely small wavelength shifts. Unfortunately, the spectrometer used in our initial demonstration does not provide sufficient resolution to take full advantage of the narrow linewidth. In our current system, we are using a compact spectrometer to measure the emission spectrum, and then using a Lorenz fitting algorithm to more accurately determine the lasing peak

wavelength. Such a strategy cannot only quantify lasing wavelength shifts in the pm range but can also reduce the complexity and cost of the detection instrument. In the future, a high-resolution laser wavelength meter based on a Fizeau interferometer (with a resolution of 0.2 pm) will be implemented. As the ECL biosensor operates in CW mode, the lasing wavelength can be accurately measured using such a wavelength meter. The relationship between the laser output power and the injection current is shown in Fig. 2(d), demonstrating a threshold current of 48 mA and a slope efficiency of 39 mW A^{-1} at 20 °C.

Results and discussion

Bulk refractive index sensitivity characterization

In order to characterize the bulk refractive index sensitivity of the sensor and to demonstrate single-mode lasing operation over a large wavelength range, PC surfaces were exposed to a series of liquid samples with the solvent dimethyl sulfoxide (DMSO) mixed with water. The refractive index (n) of the liquids ranged from 1.333 to 1.395 (at λ = 860 nm). The corresponding laser wavelength shifts (LWS) are shown in Fig. 3(a) resulting in a linear bulk refractive index shift coefficient of S_b = 212 nm/RIU over a dynamic range of 13 nm. The full operating range of the system is determined by the gain spectrum of the SOA, which has been selected to provide gain in the 830 < λ < 870 nm range.

Surface sensitivity characterization

By monitoring the spectral output of the ECL biosensor as a function of time, the kinetic characteristics of surface mass adsorption can be recorded. Fig. 3(b) illustrates the dynamic detection of the growth of a single protein polymer poly-(Lys, Phe) (PPL, Sigma-Aldrich) monolayer (thickness ~15 nm[36]) with independent wavelength measurements taken with a time interval of 500 ms. This data was obtained by initially establishing a baseline emission wavelength when the PC surface was covered with a phosphate-buffered saline (PBS) solution with pH = 7.4. After 6 min, the PPL solution was added (0.5 mg ml^{-1} in PBS) and stabilized for 20 min, followed by rinsing of the surface with PBS to remove any PPL that was not firmly attached. PPL has been demonstrated to form a self-limiting single monolayer coating upon dielectric surfaces.[36] The sensor exhibited an emission wavelength shift of ~1.24 nm for PPL monolayer adsorption, and no drift of the lasing wavelength was detectable over time periods up to one hour.

Small molecule detection

One of our goals is the detection of drug or drug-like low molecular weight molecules interacting with immobilized protein targets in the context of pharmaceutical screening, as modern drug discovery relies largely on high-throughput screening for the initial identification of candidate small molecules. A conventional demonstration for characterizing the ability of a sensor to observe small molecule binding is the detection of biotin (Molecular weight (MW) = 244 Da) by an immobilized capture layer of protein streptavidin (SA, MW = 60 kDa), given the strong binding affinity ($K_d = 10^{-15}$ M) of this interaction.[47] Such a proof-of-concept demonstration was performed on our ECL biosensor platform, with the assay protocol described in the ESI.[†] The dynamic binding curve of the biotin-streptavidin interaction is shown in Fig. 4. Any physical effect in the sample, sensor, or

detection instrument that can generate a shift of ECL wavelength that is not due to the binding of the analyte is considered as a potential error source. The most common sources of assay error for label-free biosensors are nonspecific binding and bulk refractive index variability. Common-mode error sources such as these can be largely eliminated through the use of a negative experimental control by performing the assay within adjacent "active" and "reference" microplate wells. Both the active and the reference wells are initially functionalized with a high density glutaraldehyde layer (GA, MW = 100 Da; Sigma-Aldrich), which serves as a bi-functional linker to immobilize the capture protein to the sensor surface. The capture protein is added to the active well, and allowed to bind to the GA surface. Excess (unbound) capture protein is removed from the well by a washing step with buffer. For both wells, a stable baseline is established by filling the well with 30 μL PBS buffer solution, followed by the introduction of 30 μL small molecule solution (250 ng mL^{-1} in PBS buffer) into the well. Biotin binding produced a LWS of ~23 pm on the streptavidin surface, while in the control well no binding signal was observed. For kinetic measurement of an individual sensor without referencing or temperature control, small fluctuations in the ECL wavelength are observed with a magnitude of ~4 pm, which will be discussed more fully as we address fundamental sources of sensor noise.

With this demonstration of small molecule binding in hand, the ECL sensor platform was next used to detect a more clinically relevant ligand–protein interaction in the form of estradiol and estrogen receptor α (ER). The estrogen receptors serve a variety of functions in the body and have been implicated in a range of diseases including breast cancer, osteoporosis, and atherosclerosis.[48] The molecular weights of estradiol (272 Da) and ER (63 kDa) are similar to those of biotin and streptavidin, but the binding affinity (K_d = 0.1 nM) is 10^5 times lower. Importantly, this interaction has been previously studied in optical biosensor systems, though not in a format that is compatible with high-throughput.[49] As in the biotin-SA assay, the sensor surface was functionalized with a layer of ER resulting in an LWS of 2.10 nm. Estradiol (PBS, 1% DMSO, pH 7.4) was then introduced to the ER-functionalized surface. Dynamic binding of estradiol to the immobilized ER is shown in Fig. 5(a). The expected LWS from estradiol binding is 9.07 pm, a calculated value based on the molecular weight ratio of estradiol/ER and a 1 : 1 binding stoichiometry. The experimentally measured signal agreed well with the theoretical prediction, as shown in Fig. 5(b). For all three ligand concentrations, consistent LWSs were measured as expected for all concentrations greater than K_d (0.1 nM).

DNA hybridization process study

A further demonstration of biomolecular interaction detection with binding affinities representative of biological systems, PC surfaces were functionalized with synthetic 20-mer single-strand DNA oligonucleotide probes subsequently exposed to complementary DNA oligonucleotide targets to kinetically monitor the hybridization process. The sensor was monitored continuously during the entire sequence of capture probe immobilization, washing, and hybridization as shown in Fig. 6(a). Before introducing DNA capture probes, the sensor surface was functionalized with a high density of glutaraldehyde (GA) using the same procedure described for the biotin-SA experiment. After GA functionalization, the sensor microplate well was partially filled with a 30 μL saline–sodium citrate (SSC) buffer

solution (0.045 M sodium citrate, pH ~ 7.0, 0.45 M NaCl, Sigma-Aldrich) to establish a stable baseline. Immobilization of the DNA capture probes (5′-ATT TCC GCT GGT CGT CTG CA-3′) was initiated by addition of 30 μL 4 μM concentration of the molecule in SSC buffer solution to minimize laser wavelength shift occurring through change in bulk refractive index. As a result, the in-well concentration of the DNA probes is 2 μM. At the 5′ end of the DNA probes, a tail of 12 amine groups facilitates binding of the DNA to the GA surface *via* covalent bonds. The sensor was incubated in the probe DNA solution for approximately 60 min, allowing the lasing wavelength to saturate at a stable value, followed by rinsing the sensor surface three times with SSC buffer solution to wash off any unbound DNA. In order to prevent the nonspecific binding between the target DNA and the GA surface, a blocking step using ethanolamine (EA, 200 mM) was performed to chemically react with any remaining aldehyde groups on immobilized GA molecules. We observed an initial rapid increase in lasing wavelength due to the greater refractive index of the blocking solution, followed by a more gradual negative wavelength shift during the blocking process, as loosely bound GA molecules and DNA probes were removed from the PC surface. Following a second rinse step in SSC buffer to remove the blocking solution, a stable baseline was established by adding 30 μL SSC buffer solution to the well. The 30 μL target single-strand DNA solution with a complementary sequence to the probe DNA (3′-TGC AGA CGA CGA GCG GAA AT-5′) was pipetted into the well. For this experiment, six separate biosensor microplate wells were prepared in order to separately evaluate six target DNA concentrations with three replicate wells for each concentration. The binding of target DNA was monitored for over one hour, allowing the laser wavelength shift to equilibrate to a new stable value, followed by a third rinse in SSC buffer to remove any unbound DNA. Significantly, the entire sensor preparation, probe immobilization, and target hybridization process was monitored with the smallest increment in laser wavelength shift of 0.08 pm observed. This is a consequence of the low gain ripple of the SOA, and the 2 m length of the external cavity that provides a 0.08 nm gap between allowed modes. A plot of the target DNA binding phase of the process is shown for all the analyte concentrations in Fig. 6(b).

Discussion

These initial demonstrations of the operation of an ECL biosensor highlight the aspects of detection instrument design that must be considered if one is to take advantage of a system with an extremely high *Q*-factor. First, in order to detect the smallest possible wavelength shifts that occur due to biomolecular binding, the system must not hop between modes in a discontinuous manner; thus, the system must have mode spacing less than the smallest measurable increment in wavelength shift. For the ECL biosensor, this aspect is addressed through the use of a 2 m optical fiber cavity that provides mode spacing of 0.08 pm. Second, and perhaps most importantly, experimental artifacts that generate a wavelength shift that is not due to biomolecular binding must be carefully controlled or compensated. For optical biosensors, the effects of temperature upon the refractive index of the liquid test sample, the sensor structure, and the detection instrument are the most common causes of experimental error.

Typically, commercially available NIR tunable external cavity lasers have achieved 1–2 pm short-term stability and ~50 pm long-term stability.[50,51] Although the SOA is mounted into

a package that enables temperature monitoring and closed-loop thermal control, temperature fluctuations will occur as the system responds to changes in the external environment. During the "stable" phases of the kinetic binding experiments, we observe a standard deviation of laser wavelength shifts of ~1.2 pm, which is obtained without any effort to control the temperature of the sensor, the lab environment, or the assay liquids (other than to leave them in the lab at room temperature during the experiment). Therefore, the LWS fluctuation observed is typical for that obtained for tunable ECL systems that are not used for biosensing.

Using a single active sensor at a time without a reference sensor, the ECL biosensor resolution performance is mainly limited by thermal noise. Ambient temperature fluctuations have two effects on the sensor system: (1) induction of a shift in the gain profile of the SOA, and (2) modulation of both the dimensions (through the effects of thermal expansion) and the refractive index (through the effects of the temperature coefficient of refractive index) of the PC materials. Our measured lasing wavelength value (LWV) stability for the ECL biosensor system with the sensor surface exposed to a water medium with no thermal control demonstrates a standard deviation of $\sigma = 1.2$ pm, with a fluctuation range of ~5 pm. Because the sensor surface is entirely comprised of PC, and because the microplate format enables a reference well to be placed in close physical proximity to an active well, many of the effects of common mode thermal noise may be compensated. As shown in Fig. 7(a), a reference sensor that is close to (1000 μm away from) an active sensor will undergo the same thermally induced wavelength shifts regardless of whether the cause of the variability was the SOA temperature or the PC temperature. Alternating rapidly between the two sensors and simple subtraction of the reference LWS from the active sensor LWS results in a standard deviation of $\sigma = 0.39$ pm.

Although compensation *via* a reference sensor is effective, it is even more desirable to eliminate intrinsic sources of noise. The plastic-based PCs used in this work are vulnerable to thermal fluctuations due to relatively large coefficient of thermal expansion (CTE, $\%/\Delta T$) and thermal-optic coefficients (TOE, $\Delta n/\Delta T$). For example, the TiO_2 dielectric coating has a CTE = 9.1×10^{-6} and TOE = -2.3×10^{-5} at room temperature while the UV-curable polymer layer has CTE = 50×10^{-6} and TOE = -2.8×10^{-4}. The water media in contact with the biosensor also has an intrinsic TOE = 8×10^{-5} that cannot be eliminated by sensor design. We used rigorous coupled-wave analysis[52] (RCWA) simulations to study the PC response to the effects of a small sensor temperature change upon the laser emission wavelength. Using the CTE and TOE values for TiO_2, UV-cured polymer, and water, our simulation results reveal that a temperature change of only 0.05 °C, starting at a baseline temperature of 20 °C, results in a ΔLWV of up to 5 pm, which is dominated by the high CTE and TOE of the polymer. The situation is somewhat complex, as the effects of CTE and TOE partially counteract each other, and can occur experimentally with different time dependencies. Thus, employing a substrate with much lower CTE and TOE can significantly improve the thermal stability. Quartz, for example, provides superior thermal stability, with a low CTE = 0.33×10^{-6} and TOE = $-2\ 6\ 10^{-5}$. To demonstrate improved device stability, we fabricated a PC biosensor on a fused quartz substrate using electron-beam lithography to pattern the grating structure. (See ESI[†] for fabrication details.) The quartz-based PC has a

period and grating depth identical to that of the plastic-based sensor, but with slightly different TiO_2 thickness (t_{TiO2} = 90 nm) to yield a surface that provides a resonant reflection at a wavelength near λ = 855 nm when covered with water. For this device, even without the use of a reference sensor, our stability study reveals a standard deviation of σ = 0.31 pm with a fluctuation range ~2 pm over a 6-minute time interval, as shown in Fig. 7(b).

Finally, it should be noted that, regardless of the narrowness of the resonance, high *Q* sensors will only meet their full sensing potential with highly optimized surface chemistry and functionalization techniques that support subsequent quantitative analyses. Theoretically, high stability and narrow line-width are among the key requirements for resonator-based high resolution label-free biosensing techniques. For our ECL sensor system, and for most resonator-based sensor systems, the ultimate limit of detection is set by the wavelength/frequency noise and wavelength/frequency drift level. In theory, the linewidth of the ECL system is given by the Schawlow-Townes formula (as shown in the ESI[†]) and is therefore very narrow. In reality, however, a number of phenomena have an effect on the laser wavelength. Laser current noise, for example, causes fluctuations of the refractive index of within the laser diode itself and changes the overall optical length of the laser resonator. Acoustic noise and mechanical vibrations have direct effects on the mechanical length of the external cavity, while temperature, air pressure and humidity fluctuations cause lasing wavelength drift by changing the refractive index of the optical fiber, the components of the photonic crystal filter and the sample solution, as discussed previously. Our study of the sensor's stability reveals a standard deviation of laser wavelength shifts of 0.39 (1σ) pm with referencing and 0.31 (1σ) pm using a quartz device. These correspond to wavelength shift detection resolution of 1.17 pm (3σ, with referencing) and 0.91 pm (with quartz), respectively. The demonstrated detection resolution along with the sensor's high sensitivity enable the sensor system to perform the detection of small molecules binding to immobilized protein targets below the K_d value, as discussed in the estradiol–estrogen receptor (ER) binding experiment described in the ESI.[†]

Conclusion

In conclusion, we have demonstrated a fundamentally different approach to the problem of achieving high *Q*-factor resonance and simultaneously high-sensitivity for a label-free resonant optical biosensor. Utilizing optical gain from a semiconductor optical amplifier, we use the stimulated emission process to generate extremely narrowband optical output by incorporating a PC resonator surface as the tunable element of an external cavity laser. The PC resonator reflects its energy back into the semiconductor amplifier at a wavelength that is tuned by the adsorption of biomaterial on the PC surface. This form of coupling is very robust, as the SOA and PC communicate with each other *via* an optical fiber, which is permanently coupled to the SOA package at one end and arranged for normal incidence illumination of the PC at the opposite end. We have demonstrated single-mode operation of the PC-ECL system tuned over a broad range of wavelengths, and smooth tuning between wavelengths. The ECL biosensor design separates the gain medium from the sensing transducer. In this way, the external gain becomes a permanent, unbleachable, part of the system. Such a gain separation strategy enables the transducer to be inexpensively fabricated using roll-to-roll fabrication techniques in plastic materials or upon a glass surface using a

single lithography step, and for the sensor to be operated for long time periods without degradation. The transducer itself can comprise the entire bottom surfaces of standard microplates, a capability that is several orders of magnitude beyond the throughput capabilities of any other laser biosensor approach. Finally, the ECL laser biosensor design takes the inherent advantage of external cavity laser over other lasers: much narrower theoretical linewidth. The advantages of such a system have been responsible for the wide adoption of tunable ECL lasers in the field of optical communication, and we are applying these principles for the first time in the field of biosensing. We have demonstrated the use of the system to detect an adsorbed protein thin film, the binding of small molecules to immobilized large proteins, and selective detection of DNA using an immobilized capture strand of DNA. Further, we have explored factors that impact upon the ability of the system to detect wavelength shifts less than 1 pm, demonstrating the advantages of utilizing a reference sensor and the utilization of PC materials with low thermal expansion and low thermal coefficient of refractive index. In future work, we plan to incorporate more effective methods for accurate laser wave-length measurement and sensor referencing that will further improve the system's signal-to-noise ratio, and to explore applications such as direct detection of viral particles and detection of miRNA disease biomarkers.

Supplementary Material

Refer to Web version on PubMed Central for supplementary material.

Acknowledgements

The authors gratefully acknowledge the National Science Foundation (CBET 1132225), National Institutes of Health (5R21EB009695-02 and 5R01GM90220-6) for providing financial support for this work. The authors would also like to thank the staff of the Micro and Nanotechnology Laboratory and colleagues from the Nano Sensors Group and Laboratory for Optical Physics and Engineering for their suggestions and input.

References

1. Stenberg E, Persson B, Roos H, Urbaniczky C. J. Colloid Interface Sci. 1991; 143:513–526.
2. Striebel C, Brecht A, Gauglitz G. Biosens. Bioelectron. 1994; 9:139–146. [PubMed: 8018315]
3. Özkumur E, Needham JW, Bergstein DA, Gonzalez R, Cabodi M, Gershoni JM, Goldberg BB, Ünlü MS. Proc. Natl. Acad. Sci. U. S. A. 2008; 105:7988–7992. [PubMed: 18523019]
4. Piehler J, Brecht A, Gauglitz G. Anal. Chem. 1996; 68:139–143. [PubMed: 21619229]
5. Jenison R, Yang S, Haeberli A, Polisky B. Nat. Biotechnol. 2001; 19:62–65. [PubMed: 11135554]
6. Fattinger C, Koller H, Schlatter D, Wehrli P. Biosens. Bioelectron. 1993; 8:99–107.
7. Schneider BH, Edwards JG, Hartman NF. Clin. Chem. 1997; 43:1757–1763. [PubMed: 9299972]
8. Cross GH, Reeves A, Brand S, Swann MJ, Peel LL, Freeman NJ, Lu JR. J. Phys. D: Appl. Phys. 2004; 37:74–80.
9. Freitag S, Trong IL, Klumb L, Stayton PS, Stenkamp RE. Protein Sci. 1997; 1997:1157–1162. [PubMed: 9194176]
10. US Pat. 4,608,344
11. Nellen PM, Tiefenthaler K, Lukosz W. Sens. Actuators. 1988; 15:285–295.
12. Lukosz W. Sens. Actuators B. 1995; 29:37–50.
13. Brandenburg A, Gomert A. Sens. Actuators. B. 1993; 17:35–40.
14. Millington RB, Mayes AG, Blyth J, Lowe CR. Sens. Actuators B. 1996; 33:55–59.
15. Liedberg B, Nylander C, Lundstrom I. Sens. Actuators. 1983; 4:299.

16. Myszka DG. J. Mol. Recognit. 1999; 12:390–408. [PubMed: 10611648]
17. Rich RL, Myszka DG. J. Mol. Recognit. 2001; 14:1–21. [PubMed: 11180557]
18. Rich RL, Myszka DG. J. Mol. Recognit. 2008; 21:355–400. [PubMed: 18951413]
19. Rich RL, Myszka DG. J. Mol. Recognit. 2011; 24:892–914. [PubMed: 22038797]
20. Vollmer F, Arnold S. Nat. Methods. 2008; 5:591–596. [PubMed: 18587317]
21. Lin B, Qiu J, Gerstenmeier J, Li P, Pien H, Pepper J, Cunningham B. Biosens. Bioelectron. 2002; 17:827–834. [PubMed: 12191932]
22. Cunningham BT, Laing LL. Expert Rev. Proteomics. 2006; 3:271–281. [PubMed: 16771700]
23. Arnold S, Khoshsima M, Taraoka I, Holler S, Vollmer F. Opt. Lett. 2003; 28:272–274. [PubMed: 12653369]
24. Noto M, Khoshsima M, Keng D, Teraoka I, Kolchenko V, Arnold S. Appl. Phys. Lett. 2005; 87:223901.
25. Quan H, Guo Z. Nanotechnology. 2007; 18:375702–375707.
26. Vollmer F, Braun D, Libchaber A, Khoshsima M, Teraoka I, Arnold S. Appl. Phys. Lett. 2002; 80:4057–4059.
27. Hanumegowda NM, Stica CJ, Patel BC, White IM, Fan X. Appl. Phys. Lett. 2005; 87:201107.
28. Chao C, Fung W, Guo LJ. IEEE J. Sel. Top. Quantum Electron. 2006; 12:134–142.
29. Tee CW, Williams KA, Penty RV, White IH. IEEE J. Sel. Top. Quantum Electron. 2006; 12:108–116.
30. Yalcin A, Popat KC, Aldridge OC, Desai TA, Hryniewicz J, Chbouki N, Little BE, King O, Van V, Unlu MS, Goldberg BB. IEEE J. Sel. Top. Quantum Electron. 2006; 12:148–155.
31. White IM, Oveys H, Fan X. Opt. Lett. 2006; 31:1319–1321. [PubMed: 16642098]
32. Fang W, Buchholz DB, Bailey RC, Hupp JT, Chang RP, Cao H. Appl. Phys. Lett. 2004; 85:3666–3668.
33. Guo Z, Quan H, Pau S. Appl. Opt. 2006; 45:611–618. [PubMed: 16485670]
34. White IM, Fan X. Opt. Express. 2008; 16:1020–1028. [PubMed: 18542175]
35. Yanik AA, Cetin AE, Huang M, Artar A, Mousavi SH, Khanikaev A, Connor JH, Shvets G, Altug H. Proc. Natl. Acad. Sci. U. S. A. 2011; 108:11784–11789. [PubMed: 21715661]
36. Lu M, Choi SS, Wagner CJ, Eden JG, Cunningham BT. Appl. Phys. Lett. 2008; 92:261502–261503.
37. Kita S, Nozaki K, Baba T. Opt. Express. 2008; 16:8174–8180. [PubMed: 18545528]
38. Sun Y, Shopova SI, Wu C-S, Arnold S, Fan X. Proc. Natl. Acad. Sci. U. S. A. 2010; 107:16039–16042. [PubMed: 20798062]
39. He L, Ozdemir SK, Zhu J, Kim W, Yang L. Nat. Nanotechnol. 2011; 6:428–432. [PubMed: 21706025]
40. Crow JW, Craig JRM. Appl. Phys. Lett. 1964; 5:72–74.
41. Ludeke R, Harris EP. Appl. Phys. Lett. 1972; 20:499–500.
42. Fleming MW, Mooradian A. IEEE J. Quantum Electron. 1981; QE-17:44–59.
43. Ye, C. Tunable External Cavity Diode Lasers. 1st edn.. Wei, TK., editor. Vol. 1. Singapore: World Scientific Publishing Co; 2004. p. 63-73.ch. 4
44. Mroziewicz B. Opto-Electron. Rev. 2008; 16:347–366.
45. Ge C, Lu M, Zhang W, Cunningham BT. Appl. Phys. Lett. 2010; 96:163702–163703.
46. Superlum. Traveling wave amplifier (TWA) modules. www.superlumdiodes.com/pdf/soa372.pdf
47. Livnah O, Bayer EA, Wilchek M, Sussman JL. Proc. Natl. Acad. Sci. India Sect. B (Biol. Sci.). 1993; 90:5076–5080.
48. Nilsson S, Gustafsson JA. Clin. Pharmacol. Ther. 2011; 89:44–55. [PubMed: 21124311]
49. Rich RL, Hoth LR, Geoghegan KF, Brown TA, LeMotte PK, Simons SP, Hensley P, Myszka DG. Proc. Natl. Acad. Sci. U. S. A. 2002; 99:8562–8567. [PubMed: 12077320]
50. Thorlabs. Tunable Lasers: Littrow and Littman Prealigned Kits. www.thorlabs.com/newgrouppage9.cfm?objectgroup_id=4757

51. Newport. Precision tuned lasers. http://www.newport.com/TLB-6900-Vortex-II-Lasers/984091/1033/info.aspx

52. Moharam MG, Gaylord TK. J. Opt. Soc. Am. 1981; 71:811–818.

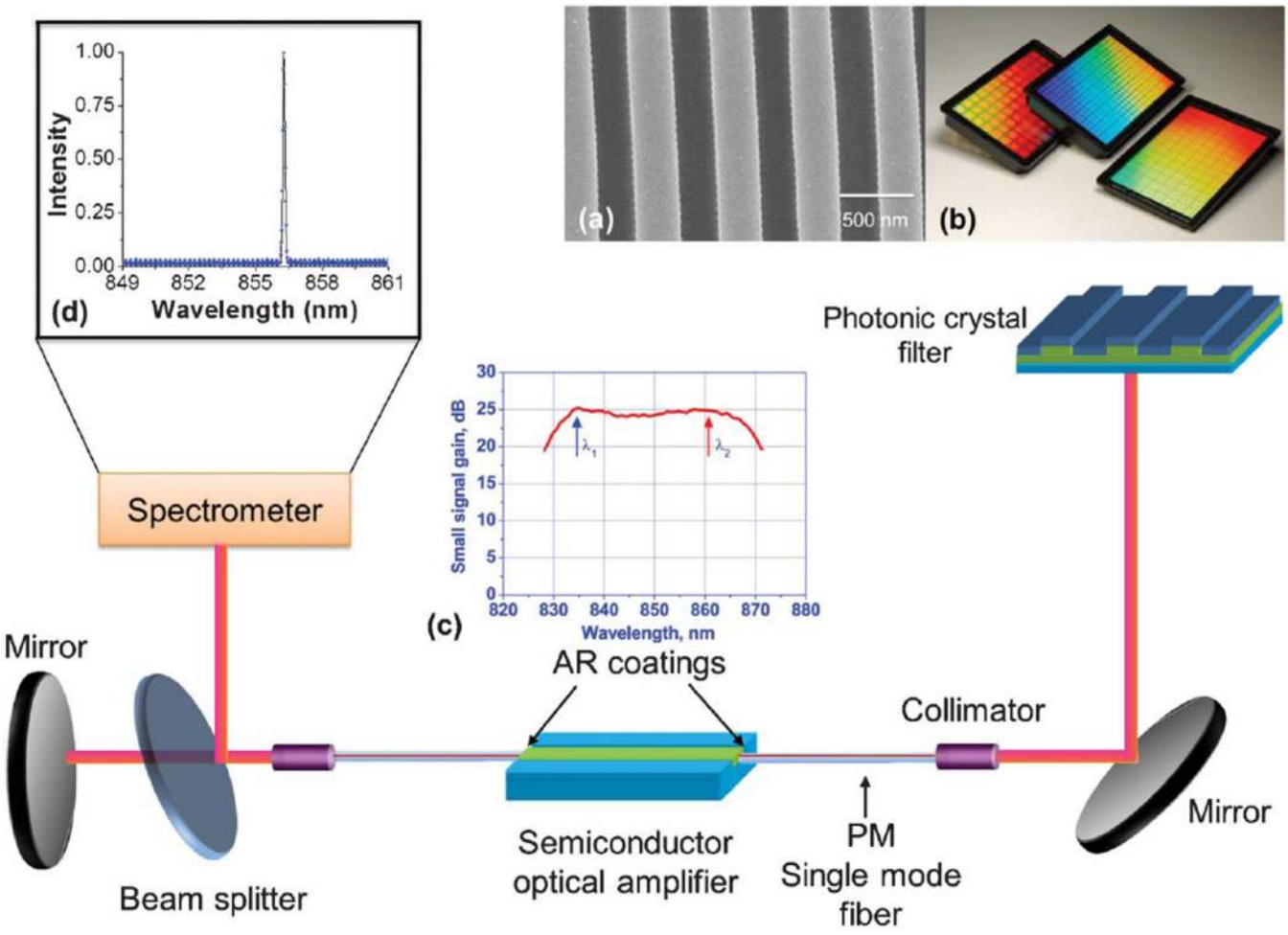

Fig. 1.

Schematic of the external cavity laser biosensor system. Inset a: Cross-section scanning electron micrograph (SEM) image of the PC structure fabricated by the nanoreplica molding process. Inset b: PC resonators in standard microplate-based format. Inset c: The small signal gain spectrum of the SOA. Inset d: Atypical lasing spectrum of the PC-based ECL.

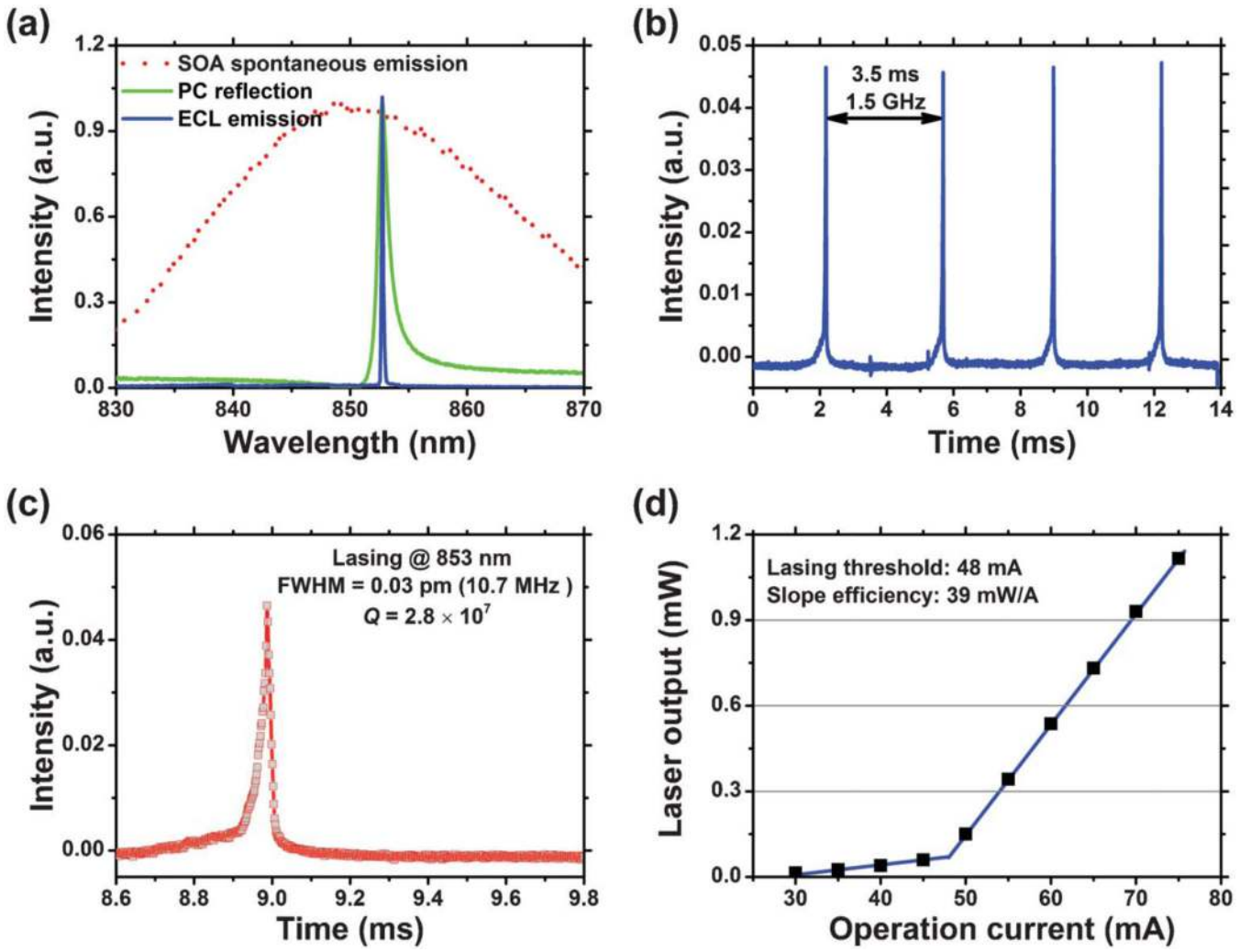

Fig. 2.

Lasing characterization. (a) Overlaid SOA spontaneous emission spectrum, PC resonant reflection spectrum, and ECL single-mode emission spectrum. The red dotted curve displays the spontaneous emission spectrum of the SOA obtained under an injection current of 56 mA at 20 °C. The green curve represents the PC resonant reflection spectrum and the blue curve denotes the ECL lasing spectrum. (b) (c) Interferogram. ECL emission spectrum measured using a scanning Fabry-Perot interferometer with 7.5 MHz resolution. (b) FSR Plot. Knowing the FSR of the interferometer is 1.5 GHz, the calibration factor is found by setting 1.5 GHz = 3.5 ms (428.57 MHz ms^{-1}), the distance between the two peaks. With the oscilloscope timebase calibrated, the FWHM of the laser emission is determined to be 0.025 ms 6 428.57 MHz ms^{-1} = 10.71 MHz, which corresponds to an FWHM = 0.03 pm in wavelength. (c) This shows a close-up of the actual signal of the laser, which results from the convolution of the laser linewidth and finesse of the interferometer FP cavity. (d) The light *vs.* current (L.I.) curve associated with the external cavity laser. Using a linear least-squares fit to the emission fluence above threshold, clear threshold current of 48 mA and slope efficiency of 39 mW A^{-1} are found.

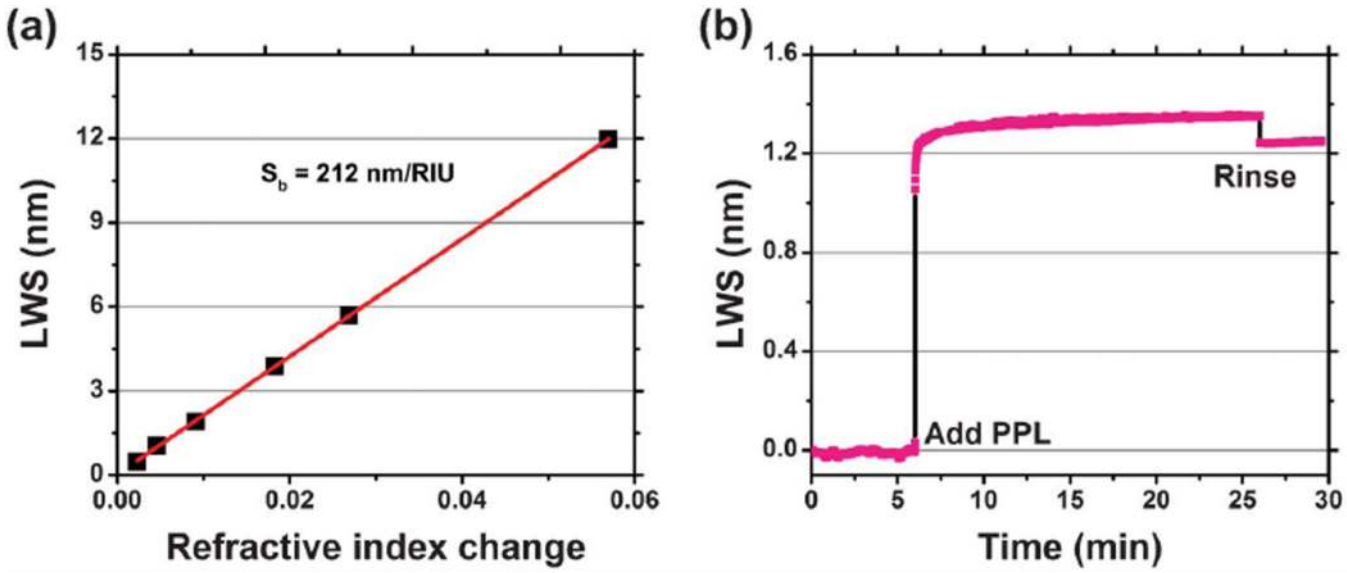

Fig. 3.

ECL sensor characterization. (a) Bulk sensitivity characterization. Laser emission wavelength shifts of the sensor exposed to liquid media with different refractive index. A linear fit to the experimentally obtained data reveals a bulk sensitivity of 212 nm/RIU. (b) Surface sensitivity characterization. Kinetic plot of polymer protein self-limiting monolayer (PPL) absorption induced laser emission wavelength shift.

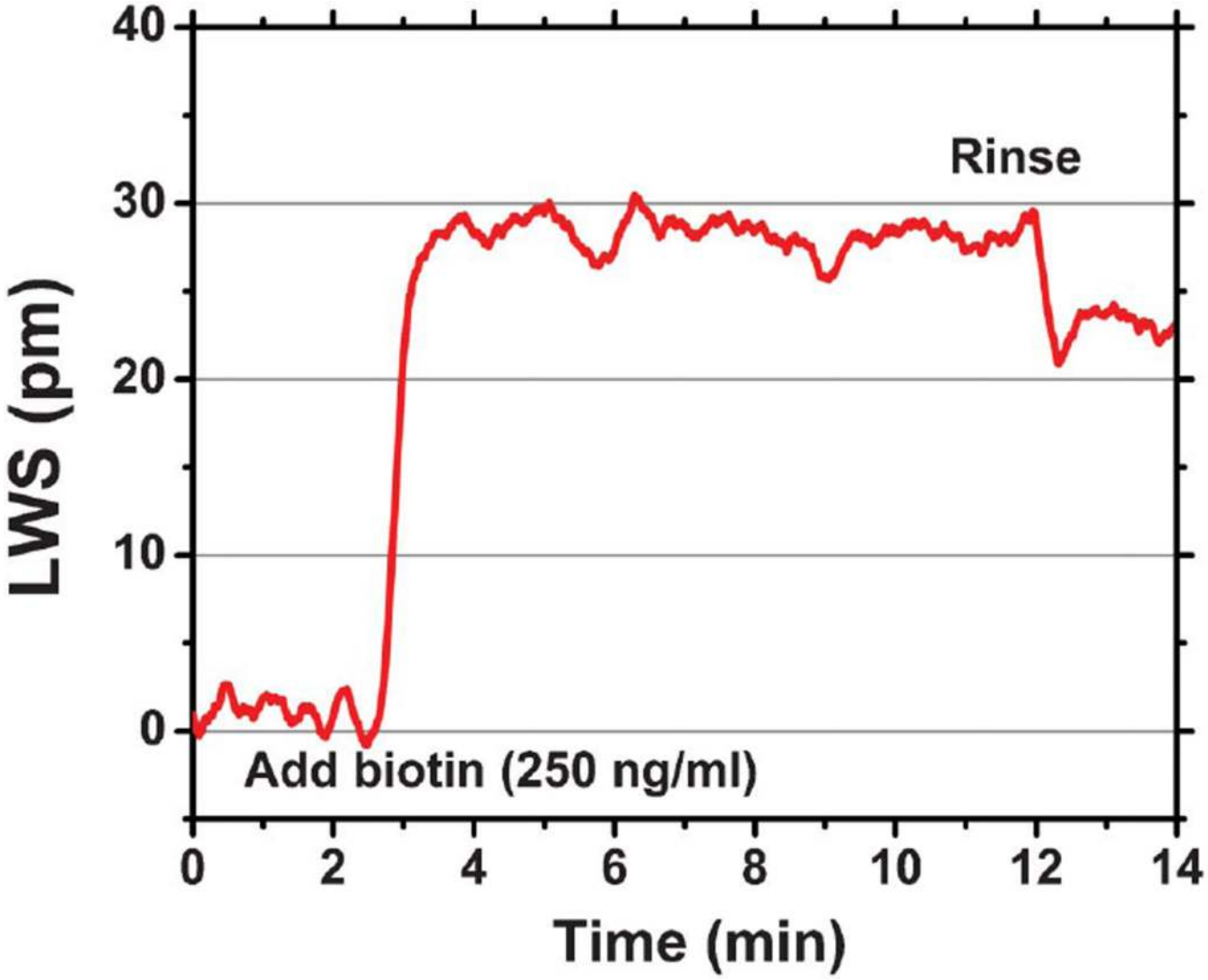

Fig. 4.

Dynamic binding of biotin to streptavidin. Lasing wavelength shift as a function of time during the exposure of a 250 ng mL^{-1} solution of biotin to the streptavidin-activated sensor.

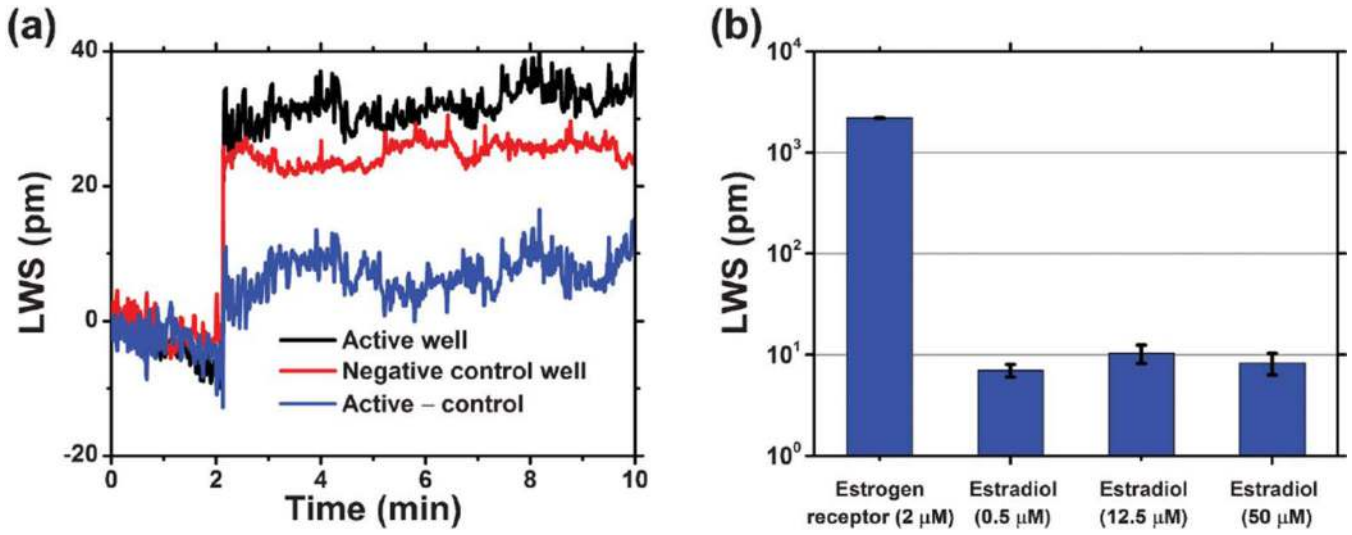

Fig. 5.

Drug-like small molecule detection: exploration of the estradiol-estrogen receptor binding. (a) Black curve represents the laser sensor's response to the addition of estradiol (50 μM in 1% DMSO solution) to the estrogen-receptor coated sensor well (half filled with PBS), while the red curve denotes the sensor's response in the control well, where the same estradiol solution was added to a glutaraldehyde-coated sensor surface (half filled with PBS). After subtracting the shifts due to the solution bulk RI change and non-specific binding, the dynamic binding of estradiol to the estrogen-receptor on the sensor's surface is shown in the blue curve. (b) Lasing wavelength shifts for immobilized ER, exposed to 0.5 μM, 12.5 μM, and 50 μM estradiol concentrations. All of the measured LWS represent the net shifts after referencing to negative controls, with error bars indicating the standard deviation of lasing wavelength values within individual sensor wells.

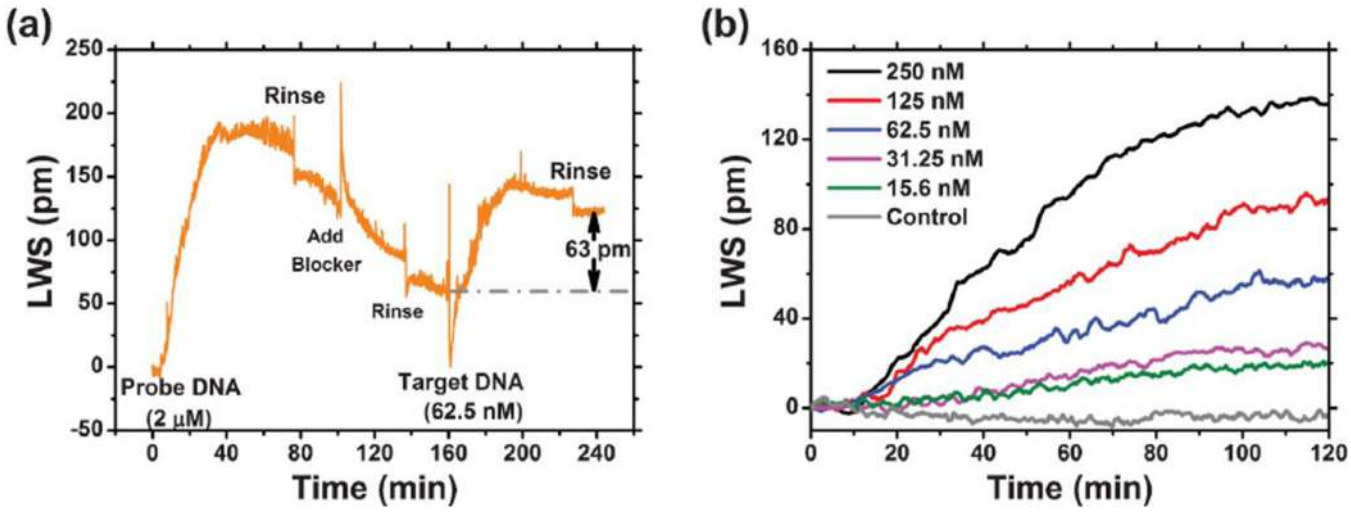

Fig. 6.

Demonstration of biomolecular interactions with binding affinities more representative of biological systems: Dynamic measurement results of the specific hybridization of complement probe DNA and target DNA molecules. (a) LWS through the probe DNA immobilization, blocker blocking, and target DNA hybridization and buffer rinsing process. (b) Selection of binding curves with varying target DNA concentrations.

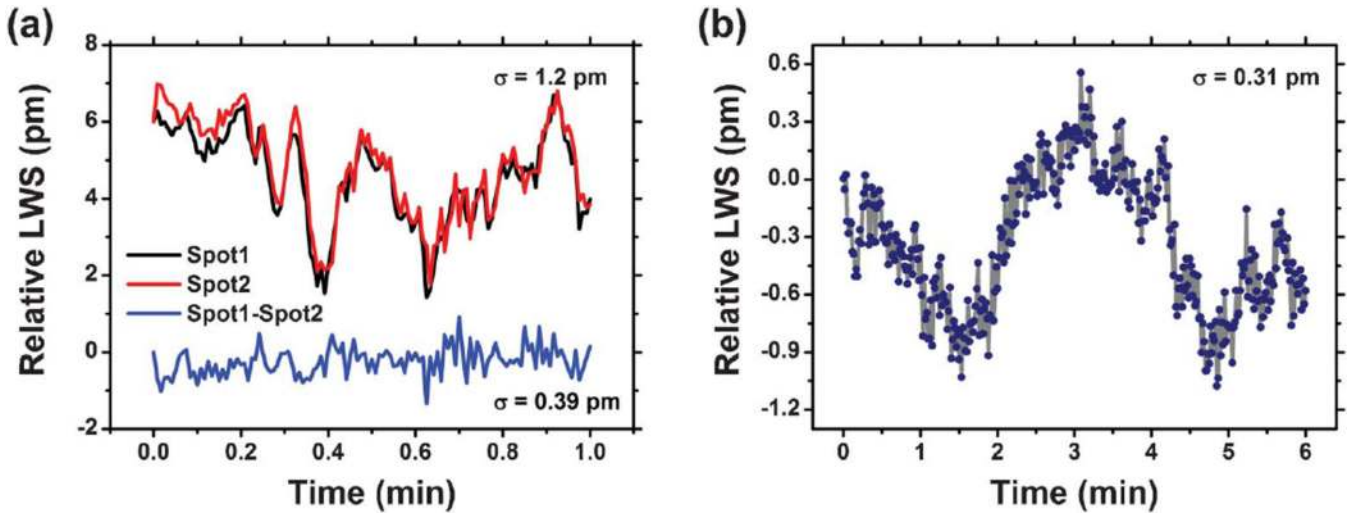

Fig. 7.

Laser emission wavelength as a function of time demonstrating the stability of the ECL system. (a) Stability measurement results obtained from a PC device fabricated on the UVCP substrate. Solid red and black curves represent the stability measurement results from two sensors with 1 mm distance. The sampling rate is 2 Hz. Alternating rapidly between the two sensors and simple subtraction of the reference (spot 2) LWS from the active sensor LWS (spot 1) results in a short-term stability of 0.39 pm (1σ), as shown in the blue curve. (b) A typical stability measurement result obtained from a PC device fabricated on fused quartz substrate. The quartz-based device has shown improved thermal immunity due to its lower TOC and CTE. A short-term stability of 0.31 pm at a sampling rate of 2 Hz for a 6-minute measurement is shown here without the need of referencing.